Illumination spectral width impacts on mask error enhancement factor and iso-dense bias in 0.6NA KrF imaging

Ivan Lalovic, Armen Kroyan, Paolo Zambon, Christopher Silsby‡, Nigel Farrar

Cymer, Inc., 16750 Via Del Campo Court, San Diego, CA 92127

‡Agilent Technologies, 4300 S. County Rd. 9, Fort Collins, CO 80528

ABSTRACT

In this study, process latitude, mask error enhancement factor and iso-dense bias have been experimentally measured as a function of the KrF excimer laser bandwidth. The experiment results are in agreement with photoresist simulations over a range of imaged nominal feature sizes from 120nm to 300nm at 0.6/0.75 NA/σ. The mask error enhancement factor (MEEF) is shown to vary by approximately 2.3% for 160nm and 3.3% for 150nm isolated lines per 0.1pm of excimer-laser bandwidth, characterized by the full width at half maximum (FWHM). The 180nm line iso-dense bias exhibits a shift of approximately 2nm per 0.1pm FWHM. Under the given process conditions, linear empirical relationships are derived for the dependency of MEEF and iso-dense offset on FWHM excimer-laser spectral width for a range of imaged CDs. Such considerations can be used to augment the existing predictive CD-control estimation and model-based optical proximity correction.

Keywords: lithography, excimer laser bandwidth, chromatic aberrations, optical proximity correction, mask error enhancement factor

I. INTRODUCTION

Critical feature dimensions in integrated circuit (IC) photolithography are being reduced well beyond the wavelength of exposure light. Projection of such sub-wavelength sized images results in non-linear image formation, whose intensity distribution is highly sensitive to deviations of the illumination partial coherence, numerical aperture and image plane. In addition—as a function of decreasing critical dimensions (CD)—imaging deviation of the photoresist-patterned critical dimension from nominal reticle feature size occurs, and is caused by the increasingly nonlinear image formation and photoresist response. This behavior is commonly characterized by the magnitude of a derived quantity, termed Mask Error Enhancement Factor (MEEF), which describes the amplification of the reticle CD-distribution imaged in photoresist. MEEF is an important consideration for control of the cross-field CD distribution and photomask tolerances. In addition to understanding MEEF, engineering of the reticle-CD features to counteract the systematic proximity and density induced image deviations, through optical proximity and process correction (OPC), is critical for an effective CD control scheme.

Understanding all of the process and tool error contributions to lithographic patterning becomes especially important as the manufacturing tolerances are reduced. Characterization of equipment effects on the process and the interaction mechanisms enable efficient process development, manufacturing ramps and inter-facility process transfers. We have focused this work on the interactions between the spectral properties of the KrF excimer laser source and lithography projection imaging. Here we present, experimental results of a study conducted in an IC fabrication facility, to quantify the effects of excimer laser bandwidth (BW) variation on an ASIC deep-ultra-violet (DUV) photolithogrpahy process, optimized for 180nm feature imaging. In particular we focus on the effects related to design and specification of binary chrome-on-glass (COG); mask error enhancement factor and iso-dense (proximity) bias. Additionally, we conduct photoresist simulations to obtain quantitative comparison with the experiment findings and verify our understanding of the interaction mechanisms.

21st Annual BACUS Symposium on Photomask Technology, Giang T. Dao, Brian J. Grenon, Editors, Proceedings of SPIE Vol. 4562 (2002) © 2002 SPIE · 0277-786X/02/$15.00

II. EXPERIMENT SETUP

2.1. Equipment and Process

The photolithography exposures in these experiments are performed statically, on the Nikon NSR-EX14C step and repeat projection system. All exposures use the full 22x22mm square field, with a variable numerical aperture (NA) and partial coherence. The maximum 0.6NA and conventional illumination 0.75σ (partial coherence) are used for all of the bandwidth imaging experiments. The illumination light source is a Cymer ELS-5400 Krypton-Fluoride (KrF) laser with 10-Watt optical output power, operating at 1kHz-pulse repetition rate.

The exposure system is interfaced with an in-line DNS-80B track supporting two spin-cups and two develop-cups, edge-expose units and multiple hot/cold plates for optimal throughput. For the purposes of this experiment, however, the track photoresist/develop process is configured for single-source processing, which means that all wafers are processed with the identical spin-cup, develop-cup and hot/cold plate units. Although this limits somewhat the wafer throughput, several sources of photoresist processing variation are removed. The photoresist process in this work is a modification of an existing gate lithography process for 220nm CMOS device manufacturing—optimized for 180 - 200nm feature geometries. Shipley's UV5 photoresist is used with a casting thickness of 5000Å. The photoresist soft bake temperature is 135ºC applied for 60-seconds; the post exposure bake (PEB) temperature is 130ºC for 90seconds. The AR2 bottom anti-reflective coating (BARC) also manufactured by Shipley is applied to minimize thin-film interference effects, with thickness of 600Å baked at 205ºC for 60seconds. Standard 0.26N TMAH single-puddle developer is used without surfactant, with puddle time of approximately 46sec. The substrates are bare-silicon 8" wafers pre-sorted for minimal global and local flatness deviations, therefore all wafer measurements are of post-develop photoresist features.

In this work, we investigate critical dimensions ranging from 120nm to 300nm, imaged using a standard 6" binary chrome-on-glass (COG) test reticle, containing multiple feature dimensions and configurations. The process latitude effects are evaluated for 180nm lines. Where available, measurements of the reticle features allow correction of the wafer measurement results, which is especially critical for evaluation of photoresist linearity and MEEF. The dose-to-size range for the features and process given above is between 14mJ/cm^2 and 19mJ/cm^2. Each experimental wafer consists of multiple fields exposed at different dose and focus settings; what is commonly referred to as focus-exposure matrix (FEM). The distance between lateral steps of the FEM is 1mm on the wafer minimizing the effects of substrate nonflatness.

2.2. Metrology and Experimental Adjustments

Two laser parameters are varied in the experiments presented here: spectral bandwidth and central wavelength. The central wavelength output of the excimer laser can be modified via software control of the line-narrowing module (LNM) optics. The wavelength set point is accessed though the user interface on the laser handheld keypad (also called *paddle*); this is a relatively fast adjustment performed in the laser idle state. In addition, the laser system enables accurate calibration of the KrF wavelength, using the AWR (absolute wavelength reference) technique, based on Iron (Fe) lamp absorption. During normal operation of the laser, the wavelength of light is actively controlled. In this work, the nominal set-point wavelength is 248.3850nm. On this system, the laser spectral width is modified manually by adjustment of the line-narrowing optics in the LNM. The full-width-at-half-maximum (FWHM) of the spectrum is varied from 0.41pm to 1pm and is measured using the on-board wavemeter etalon device. We refer to the minimum bandwidth (BW) setting of 0.41pm as nominal condition for this sytstem. Previously, we have discussed the importance of characterization of spectral bandwidth using the 95% energy integral width (E95%),[1] however, metrology techniques for accurate measurement of the entire illumination spectral profile are not used in this work.

The CD metrology in this study is carried out using top-down scanning electron microscopy (SEM) with the Hitachi 8840 automated CD SEM. As mentioned previously, the majority of wafer CD measurements are corrected for reticle CD errors. The focal position of the projection lens is characterized using the in-situ sensor and wafer-based self-diagnostic systems available on the exposure system. The wafer-based self-diagnostic focus is determined from the photoresist feature response to de-focus at five locations within the static field.

III. LITHOGRAPHY MODELING

In this study, the impact of laser bandwidth on photoresist imaging is also studied using lithography simulation based on the PROLITH/2 computation package.[2] The inclusion of the spectral extent of the excimer laser is accomplished by principle of weighted superposition. The aerial image intensities are weighted by the corresponding spectral intensities and are added together to obtain the resulting image. Simulation approaches, proposing incoherent image interaction at the wafer plane, have been demonstrated previously.[3] The illumination spectrum input for the simulation is based on high precision double-pass grating spectrometer measurements of comparable 1kHz systems. In the present work, the lithography model assumes that only the focus aberration changes as a function of wavelength. The wavelength-defocus relationship is characterized by a linear response of 250nm defocus per 1pm of wavelength offset or 0.25ppm (parts per million); the measurement of this behavior is discussed below. Although other aberrations have been shown to vary with wavelength, the simplified approach is consistent with high precision in-situ chromatic aberration measurements reported previously for exposure systems of similar type.[4,5]

A refined model of the UV5 photoresist performance is developed matching closely the physical photoresist and developer recipe settings. The simulation results are analyzed to estimate the exposure latitude, MEEF as well as response of isolated and dense line structures. As discussed in the following section, the use of simulations in this study enables confirmation of the experimental results as well as quantification of effects beyond those tested in experiments.

IV. RESULTS DISCUSSION

4.1. Longitudinal Chromatic Aberration

The change of the focal plane as a function of wavelength offset was measured for two NA settings, *0.6NA and 0.5NA*, on the exposure system. The wavelength of the laser is adjusted over a 6pm range and the best focus at five points across the field is shown in Figure 1 below.

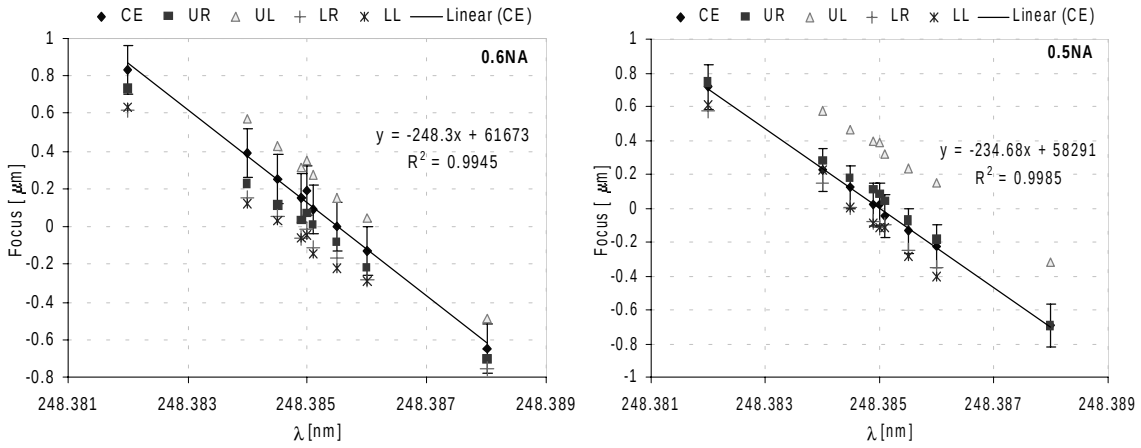

Figure 1. Longitudinal chromatic aberration for 0.6NA and 0.5NA

Here, the five field locations are denoted: center-CE, upper right-UR, upper-left-UL, lower right-LR, lower left-LL, corresponding to the center and the four corners of the static field. The data is described by a linear fit, where the slope quantifies the focus sensitivity to wavelength. The wavelength-defocus relationship is also termed longitudinal chromatic aberration, since the variation is along the optical axis. In Figure 1, the CE data is shown fitted with the least squares approximation, the resulting line equations and R^2 residuals are displayed. For this system, the results indicate approximately 250nm of focus shift per 1 pm of wavelength offset for 0.6NA and is consistent with previously published results.[4,5] The R^2 values range from 0.993 to 0.999, showing very good linearity across the 6pm wavelength range. The across-field focus variation is approximately 0.4μm in this result and is caused by a field leveling (software) offset, which is constant for these experiment conditions.

4.2. Bandwidth-induced Process Latitude Changes

In Figure 2, below, the measured CD-defocus behavior is shown for 180nm vertical (V) and horizontal (H) isolated lines at field center.

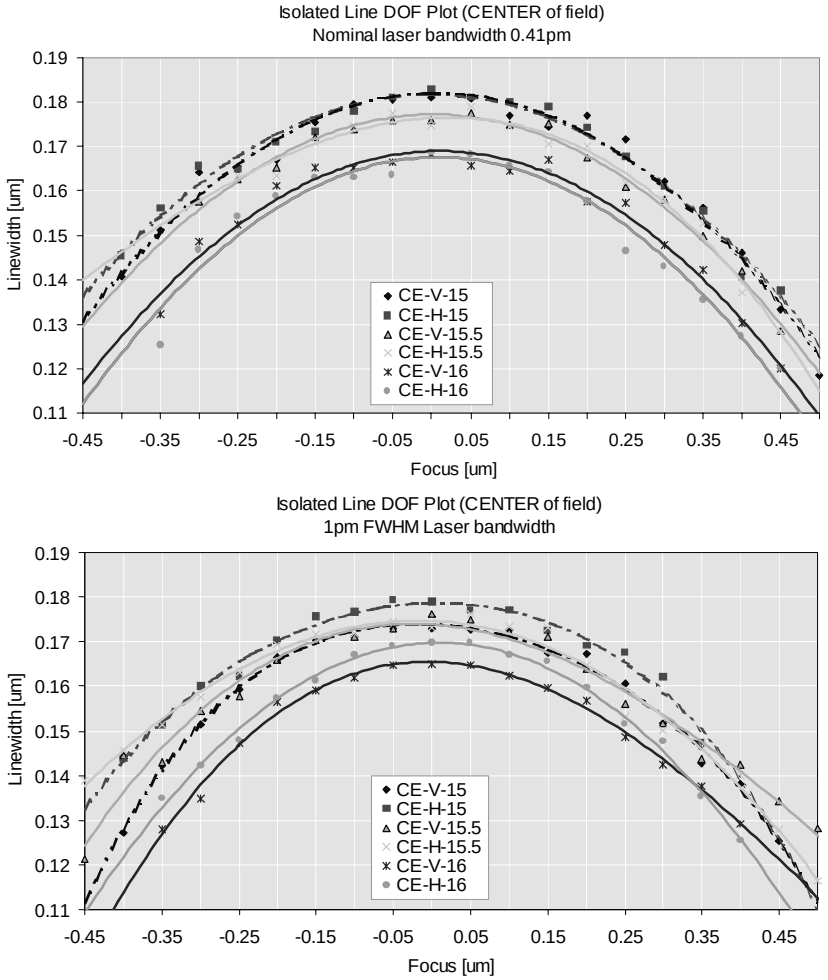

Figure 2. CD-defocus plots of 180nm isolated features for 0.41pm and 1pm FWHM spectra

The graphs in Figure 2 display the CD measurement results at three exposure dose settings 15, 15.5 and 16mJ/cm^2. Therefore, for example, data labeled CE-V-16 denotes vertical line, exposed at 16mJ/cm^2 measured at field center. All of the displayed experimental data are fitted with polynomial curves. In this case, the reticle CD error is subtracted from the SEM wafer measurements. From these graphs, we observe qualitative changes in the CD-defocus response. Primarily, we observe a negative CD bias as a function of

broadened spectrum. The isolated lines are reduced by approximately 2 to 15nm when the FWHM bandwidth is increased from 0.41 to 1pm, depending on field location and focus condition.

The relationship between exposure latitude (EL) and depth of focus (DOF) is calculated from the CD-defocus-dose data, by assuming rectangular process window with a 10% CD variance specification. The experimental process latitude as a function of bandwidth, calculated using ProDATA[2], is shown in Figure 3. The simulated process latitudes are also shown for 1pm, 0.4pm and monochromatic (0pm) bandwidth conditions.

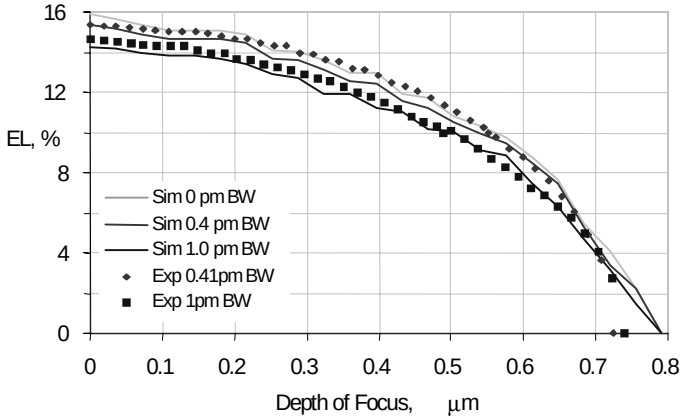

Figure 3. Simulated and experimental 180nm isolated line process latitude as a function of FWHM

In Figure 3, although a slight EL offset is present, the agreement between simulation and experiment is very good. The relative change in EL is roughly constant across the DOF range and is approximately 7% per 0.6pm FWHM difference, or 1.2% / 0.1pm FWHM. For EL between 14% and 6%, the absolute change in the DOF is relatively constant; approximately 0.1μm between the two FWHM-bandwidth conditions. The reduction of EL and the process window has been related to the calculated aerial image contrast and log-slope response to changes in bandwidth, and has been presented previously.[1,3,6]

4.3. Iso-Dense Bias, MEEF and Illumination Spectral Width

In Figure 4, we show the CD response of isolated and dense 180nm features to exposure dose setting, imaged at best focus. The response of CD to exposure dose is commonly fitted by the following empirical relationship, $CD = A + B * (Dose)^{-1}$, where *A* and *B* are the adjustable fit coefficients. The raw CD data points and the line-fits are displayed in the figure below.

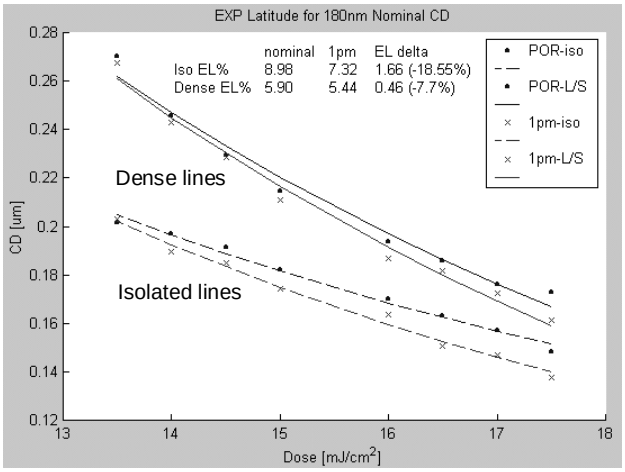

Figure 4. CD exposure-bias for 180nm dense and isolated lined; BW is 0.41pm and 1pm FWHM

The reciprocal CD-dose fit describes well the response of isolated lines; for dense lines (1:1 line-space ratio) the empirical 1/dose relationship is not as representative. From the slope of the fitted curves we calculate the relative exposure latitude at best focus and dose-to-size. The EL results are summarized in print on the graph above, showing approximately 3.1% relative EL change per 0.1pm FWHM for isolated lines. The iso EL results at best focus here differ from the process window results in the previous section due to the type of evaluation performed as well as the use of an extended exposure dose range. In this figure, we also note that isolated and dense lines have different response to exposure dose, which results in an iso-dense exposure bias. We estimate the iso-dense exposure bias to be approximately 8nm per 1mJ/cm^2 at the 15.5mJ/cm^2 dose-to-size for the nominal BW condition. At the same target dose at 1pm FWHM, the iso-dense exposure bias is approximately 9.5nm per 1mJ/cm^2. The CD data at 15.5 mJ/cm^2 is removed due to a systematic measurement offset caused by SEM-induced sample contamination.

In addition to the iso-dense exposure bias of the 180nm process, the iso-dense bias is also changes as a function of the illumination spectral width, since the aerial images of isolated and dense lines exhibit different degrees of sensitivity to spectral width. The response of the iso-dense bias to bandwidth—obtained experimentally and using simulation—is shown in Figure 5 below. Here, the iso-dense bias sign convention is given by $Bias = CD_{dense} - CD_{iso}$.

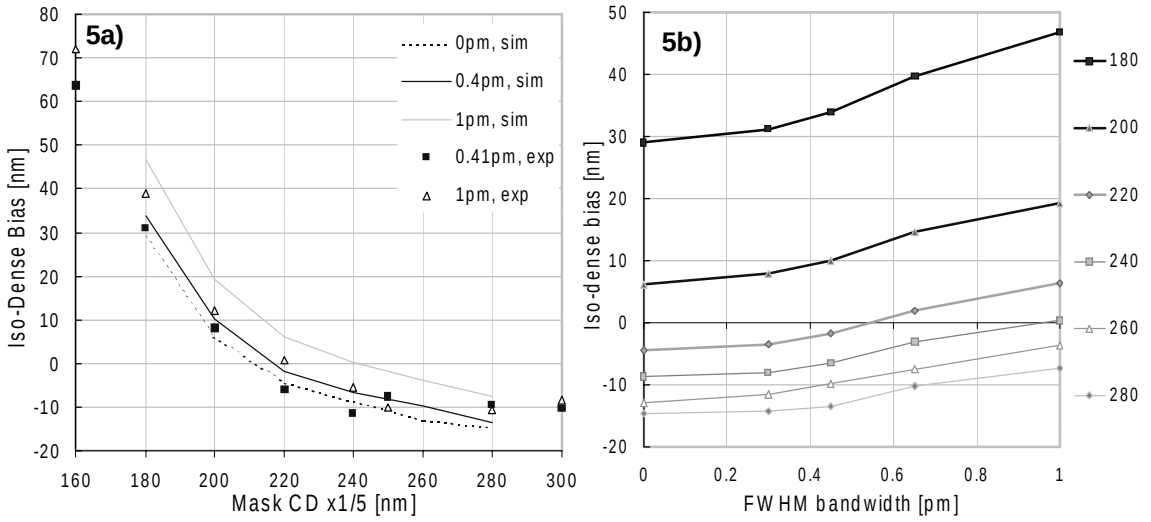

Figure 5. Iso-dense bias as a function of bandwidth *(Figure 5a and 5b)*

In Figure 5a, we show the experimentally measured and simulated iso-dense bias results for a range of nominal feature sizes. The bias is relatively well behaved for features from 300nm to 240nm however it rapidly deteriorates as feature sizes are reduced. The agreement between experiment and simulation results is very good, without considerable model tuning. However, approximately a 5nm offset is observed between simulation and experimental response to the 0.6pm FWHM change. Figure 5b, shows the simulation results of iso-dense bias as a function of FWHM bandwidth. The response in the range from 0.45pm to 1pm can be linearly approximated. For 180nm features, the iso-dense bias exhibits a shift of approximately 2.3nm per 0.1pm FWHM. The sensitivities for the other feature sizes are summarized in Table 1 below.

Nominal CD feature [nm]	***180***	***200***	***220***	***240***	***260***	***280***
Iso-dense bias change [nm / 0.1pm FWHM]	2.3	1.6	1.4	1.2	1.1	1.1

Table 1. Iso-dense bias variation

In addition to iso-dense bias—from the SEM measurements and simulations—we characterize the photoresist linearity of the printed features and calculate the mask error enhancement factor (MEEF). It is expected that the image contrast and log-slope modulation introduced by bandwidth changes will also

affect the linearity and MEEF, especially for sub-wavelength feature sizes. Since the magnitude of the BW effects is different for isolated and dense line images—which previously we show results in iso-dense bias variation—different degree of MEEF deviation is expected for isolated and dense features; however, in this work we focus on the isolated line linearity and MEEF. BW-induced MEEF changes are also expected to be strongly dependent on the feature size and imaging condition. In Figure 6 below, the measured and modeled photoresist CD linearity for isolated lines is shown; the calculated MEEF metric (first derivative of the linearity data) is also shown to the right.

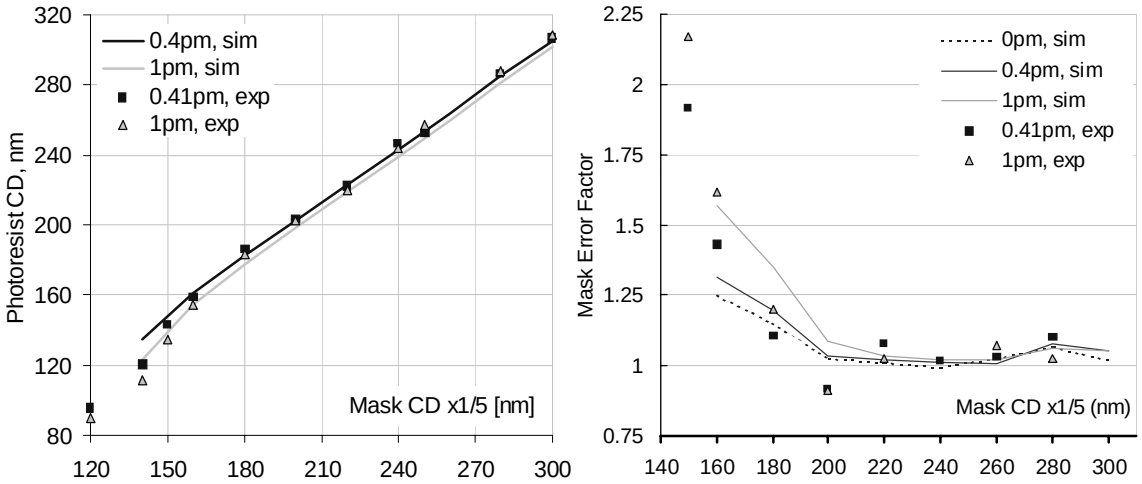

Figure 6. Simulation and experiment results: BW-induced CD linearity and MEEF variation

The experimental linearity data shows very good agreement with simulation over a range of feature sizes from 300nm to 150nm. Below 180nm (and below the 220nm specification of the imaging system) the results show deviation from a linear CD response, which reflects the diminished resolution of the smaller features at the 0.6NA maximum numerical aperture. In photoresist, even the sub-150nm isolated lines are successfully imaged however with considerable sidewall slope and line-edge roughness—quite noticeable using scanning electron microscopy. The MEEF also dramatically increases when features are reduced below 180nm. The MEEF results show that the deviation from linearity (deviation from MEEF of 1) occurs for features smaller than 180 - 200nm. Observably, as illumination spectral width is varied the MEEF also changes. The variation in MEEF per 0.1pm FWHM is expressed as a percentage of the nominal value; the results for various feature sizes are summarized in Table 2 below.

Nominal CD feature [nm]	***150***	***160***	***180***	***220***	***240***	***260***
MEEF relative change [% / 0.1pm FWHM]	3.3	2.3	0.8	0.2	0.1	-0.05

Table 2. BW-induced MEEF variation

The MEEF sensitivity to bandwidth increases as feature sizes are reduced towards the limit of image quality and reproducibility. Although in this case the BW contribution to MEEF is small at the 220nm-resolution specification of this 0.6NA exposure system, the use of lithography exposure systems in R&D and manufacturing is commonly extended well below the specified feature resolution.

V. SUMMARY AND CONCLUSION

In this work we discuss the interactions between the illumination source spectral width and the photoresist process response. The experimental and simulation results show that the source bandwidth impacts various aspects of image reproducibility: exposure latitude, depth of focus, iso-dense bias and mask error enhancement factor (and linearity). For features larger than 160nm, the iso-dense bias changes by as much as 2.3nm per 0.1pm, MEEF by 2.3% per 0.1pm and EL by 3.1% per 0.1pm FWHM bandwidth. Considering that the bandwidth variation over the lifetime of current excimer laser systems is typically

better than 0.1pm to 0.2pm, the bandwidth-induced process effects are small compared to typical random process and tool-induced errors in the lithography process of 150 – 130nm device manufacturing.

Nevertheless, continued work on understanding all of the measurable contributors to image formation enables the development of a comprehensive model of imaging in photolithography. Such understanding can be used to improve the lithography process and tool specification and design, as well as develop recursive (feed-back) and predictive (feed-forward) algorithms for automated process and equipment control. Also, in lithography, the interaction of multiple *small* components can amount to an appreciable contribution to the overall process manufacturability margin.

We have shown that MEEF and iso-dense bias sensitivity to bandwidth is affected by feature size that is being resolved. Therefore, the bandwidth sensitivities are expectedly also affected by the imaging condition (numerical aperture and partial coherence), photomask manufacture, presence of lens aberrations and flare (scattered light), photoresist process, etc. Such interaction effects can be taken into account by additional refinement of the lithography model inputs. In addition, the incorporation of bandwidth effects for comprehensive OPC design and verification can also be used to more accurately match the resulting OPC design to real-world fabrication conditions—applicable to derived OPC rules or model-based approaches.

ACKNOWLEDGMENTS

The authors would like to acknowledge the support of operations personnel at the B2 Fabrication facility in Fort Collins, Colorado as well as management of SiTD-TDC-ICBD. Assistance of Mara Konopasek with SEM metrology is also recognized.

REFERENCES

[1] A. Kroyan, I. Lalovic, N.R. Farrar, "Effects of 95% integral vs. FWHM bandwidth specifications on lithographic imaging," *Proc. SPIE Optical Microlithography XIV* **4346**, 1244 (2001).
[2] PROLITH/2 and Klarity ProDATA are registered trademarks of KLA-Tencor, San Jose, CA.
[3] A. Kroyan, J.J. Bendik, O. Semprez, N.R. Farrar, C.G. Rowan, C.A. Mack, "Modeling the effects of excimer laser bandwidths on lithographic performance," Proc. SPIE Optical Microlithography XIII **4000**, 658 (2000).
[4] M. Terry, I. Lalovic, G. Wells, A.H. Smith, "Behavior of lens aberrations as a function of wavelength on KrF and ArF lithography scanners," *Proc. SPIE Optical Microlithography XIV* **4346**, 15 (2001).
[5] I. Lalovic, A. Kroyan, N.R. Farrar, P. Zambon, A.H. Smith, "Investigation of cross-field wavefront aberrations of KrF lithography exposure systems as a function of excimer laser bandwidth," *Proc. SPIE Optical Microlithography XIV* **4346**, 1262 (2001).
[6] A. Kroyan, I. Lalovic, N.R. Farrar, "Contribution of polychromatic illumination to optical proximity effects in the context of deep-UV lithography," *presented at BACUS XXI Photomask Technology Symp.*, Oct. 2-5, 2001.